ADVANCES IN MATERIALS SCIENCE, Vol. 24, No. 4 (82), December 2024

DOI: 10.2478/adms-2024-0025

Robert Kosturek*, Tomasz Ślęzak, Janusz Torzewski

Military University of Technology, Faculty of Mechanical Engineering, Warsaw, Poland

***** *robert.kosturek@wat.edu.pl*

STRUCTURAL INTEGRITY OF AA7075-T651 UWFSW JOINTS

ABSTRACT

This investigation is focused on the comparison of selected low-cycle fatigue properties of AA7075-T651 friction stir welded and underwater friction stir welded joints together with the evaluation of their lifetime prediction by the Manson-Coffin-Basquin formula. Additionally, the analysis of the fractured surface was involved to describe the character of joints decohesion. The analysis of the obtained hysteresis loops revealed that FSW joint exhibits cyclic hardening, with a stable maximum stress and a decreasing minimum stress, leading to an increased contribution of compressive stresses and a lower mean stress during stabilized fatigue. In comparison, the UWFSW joint also shows cyclic hardening but with a greater contribution of tensile stresses, a higher mean stress, and a reduced participation of plastic deformation. The Manson-Coffin-Basquin equation effectively predicts the fatigue life of AA7075-T651 alloy joints, with UWFSW joints showing significantly lower standard deviation (0.0035 vs. 0.0135) and narrower dispersion bands (1.61 vs. 1.93) compared to conventional FSW joints.

Keywords: *aluminum; friction stir welding, fatigue, fracture, lifetime*

INTRODUCTION

Friction stir welding (FSW) enables the creation of cohesive joints in 7XXX series alloys, which are generally considered unweldable [1]. Performing the process in the solid state not only eliminates many issues associated with conventional welding processes but also positively impacts the strength properties of the joints. In recent years, numerous studies have demonstrated that applying the FSW method to join elements made from the 7075-T651 alloy in a butt joint configuration can achieve joint efficiency in the range of 60-80%, depending on the applied process parameters, tool type, and the thickness of the materials being joined [2-5]. Additionally, certain modifications of the process, such as underwater friction stir welding (UWFSW), significantly enhance the strength parameters of AA7075-T651 joints [6-8]. The use of an additional cooling medium, such as water, helps dissipate excess heat from the joined element, thereby minimizing losses in the strengthening phase of the high-strength aluminum alloy [9,10]. As a result, UWFSW joints typically exhibit higher yield strength and tensile strength compared to their counterparts produced using the conventional FSW technique [11-12]. Moreover, they feature a narrower heat-affected zone and a harder low-hardness zone [13]. In recent years, there

Received: 2024.10.15; Received in revised form: 2024.12.14; Accepted: 2024.12.16

has been significant interest in the UWFSW technique for joining non-precipitation-hardened alloys, primarily the 5XXX series alloys designed for marine structures [14]. These alloys generally exhibit good mechanical properties and high corrosion resistance, even in conventional FSW joints [15,16]. The greatest improvement in the performance properties of FSW joints is observed in underwater welding of precipitation-hardened alloys, as they are the most vulnerable to a decline in mechanical properties due to the heat generated during the joining process.

When considering the behavior of a structure containing UWFSW joints under variable load conditions, special attention must be paid to their fatigue properties. As demonstrated in several research studies, fatigue properties are also significantly improved by performing the FSW process in a water environment [13-17]. Despite understanding general trends in the fatigue behavior of FSW and UWFSW joints, the topic is still not fully explored, and the ability to predict the lifetime of such joints is continuously being developed. FSW joints are characterized by a deformed, partially dynamically recrystallized structure, with the boundaries between recrystallized, deformed, or grown grains acting as microstructural notches [18-20]. In precipitation-strengthened alloys, the non-uniform distribution of the strengthening phase within the joint further contributes to differences in strength properties between the zones [4,7,21]. Residual stresses also play a role, although it should be noted that their values are generally lower in FSW joints compared to conventional welded joints [22]. Additionally, the minimal reduction in the thickness of the joined elements in the tool shoulder's area of influence must be considered, as it creates a geometric notch in such joints.

When analyzing the behavior of the examined joints under variable stress conditions with significant amplitude, it is necessary to rely on low-cycle fatigue (LCF) models that account for the contribution of plastic deformation in each loading cycle. The Manson-Coffin-Basquin equation is often used to describe the low-cycle fatigue behavior of FSW joints [13,17,20,23], yielding good results for predicting the behavior of high-strength aluminum alloys in their as-received state as well [24]. Previous preliminary studies on the low-cycle fatigue of FSW and UWFSW joints in the AA7075-T651 alloy revealed significant differences in their behavior, in particular, that UWFSW joints exhibit a greater tendency for cyclic hardening, lower plastic strain amplitude, and fewer cycles to failure [13].

The aim of this study, as a continuation of previous research is to compare selected fatigue properties of FSW and UWFSW joints of AA7075-T651 alloy, determine the feasibility of predicting their fatigue lifetime, and identify phenomena occurring during their decohesion.

EXPERIMENTAL

The FSW and UWFSW joints under investigation were produced in a butt joint configuration using 5 mm sheets of AA7075-T651 alloy. The chemical composition (provided by the supplier, Bikar Metalle) and the mechanical properties (tested by the authors) of the sheets used are shown in Tables 1 and 2, respectively.

Table 1. *Chemical composition of 7075-T651 (% weight)*

Si	Fe	Cu	Mn	Mg	Cr	Zn	Ti	Al
0.071	0.122	1.610	0.025	2.596	0.197	5.689	0.041	Base

Table 2. *Mechanical properties of 7075-T651*

Microhardness	Yield Strength, $R_{0.2}$	Tensile Strength, R_m	Elongation at break
170 ± 3.6 HV0.1	547.5 ± 1.3 MPa	583.5 ± 1 MPa	14.4 ± 0.6%

The joining process was carried out in two variants: conventional air-cooled FSW and underwater FSW. In both cases, the following process parameters were applied: tool rotational speed of 400 rpm, tool travel speed of 100 mm/min, tool plunge depth (measured from the tip of the pin) of 4.8 mm, and a tool tilt angle of 2°. An ESAB tool with catalog number 0810134-001 was used. For the UWFSW process, a 10% solution of Blasocut 2000 was used as the cooling medium. The initial temperature of the medium was 20°C, and the liquid surface was 15 mm above the upper surface of the joined sheets. The welding process was performed using an ESAB FSW Legio 4UT machine, presented in Figure 1.

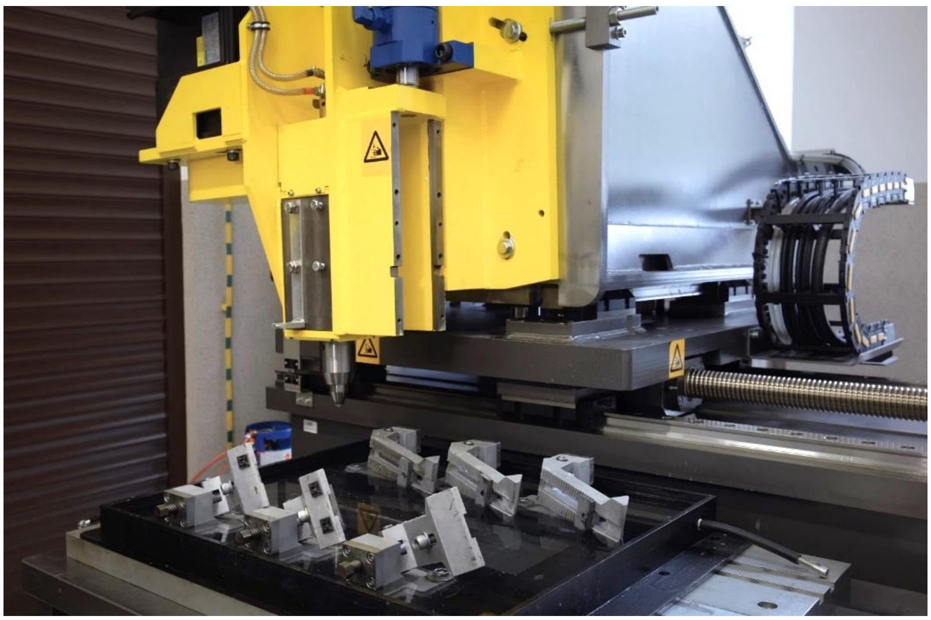

Fig. 1. ESAB FSW Legio 4UT

The macrostructure, microhardness, and basic mechanical properties of the joints produced in this manner were discussed in a previous study [13]. The basic mechanical properties of the examined FSW joints, determined through static tensile testing, are presented in Table 3.

Table 3. *Mechanical properties of investigated FSW joints*

Sample	Yield Strength, $R_{0.2}$	Tensile Strength, R_m	Elongation at break	Failure location
FSW	314.8 ± 2 MPa	447.7 ± 1.2 MPa	5.8 ± 0.3%	Thermo-mechanically affected zone
UWFSW	360.2 ± 0.7 MPa	494.1 ± 2.6 MPa	6.2 ± 0.1%	Thermo-mechanically affected zone

Fatigue tests were conducted with a cycle asymmetry ratio of R=0.1 and strain amplitudes of ε_{ac}=0.35%, 0.4%, 0.5%, and 0.6%, using an Instron 8802 MTL machine in accordance with ASTM E8/E8M–13a standards. The fracture surfaces of the failed samples were subjected to microfractographic analysis using a Jeol JSM-6610 scanning electron microscope.

RESULTS AND DISCUSSION

The hysteresis loops from the 1st, 10th, 100th, and mid-life cycles for the FSW and UWFSW joints tested at a strain amplitude of ε_{ac}=0.6% are shown in the Figure 2a and b.

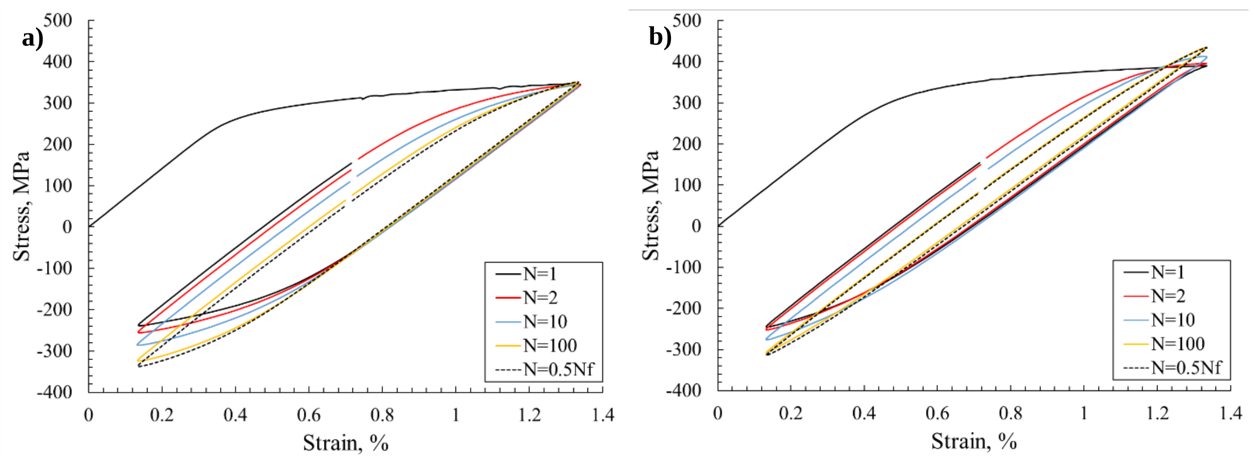

Fig. 2. Hystersis loops of FSW (a) and UWFSW (b) joints tested at ε_{ac}=0.6%

Analyzing the changes in positions and sizes of successive loops for the FSW joint (Fig. 2a), it can be concluded that the joint undergoes cyclic hardening. Additionally, the maximum stress value remains largely unchanged, while the minimum stress value decreases significantly, from σ_{min}=230 MPa at N=1 to σ_{min}=340 MPa at N=0.5N_f. With each subsequent cycle, the contribution of compressive stress increases, and the mean stress value during the period of stabilized fatigue properties reaches about σ_m=50 MPa. For the UWFSW joint (Fig. 2b), comparing the loops at N=1 and N=0.5N_f, an increase in maximum stress (from 390 MPa to 435 MPa) and a decrease in minimum stress (from 245 MPa to 320 MPa) are observed. Compared to the conventional FSW joint, the UWFSW joint exhibits a greater contribution of tensile stresses at the analyzed total strain amplitude, with the mean stress value during property stabilization reaching approximately 90 MPa. Additionally, in this case, a tendency for cyclic hardening of the specimen is observed. However, the area of the mid-life loop for the analyzed joints indicates a noticeably lower contribution of plastic deformation in the UWFSW joints. In a previous article published by the authors [13], the low-cycle fatigue behavior of FSW and UWFSW joints was presented on a Manson-Coffin-Basquin plot (Fig. 3).

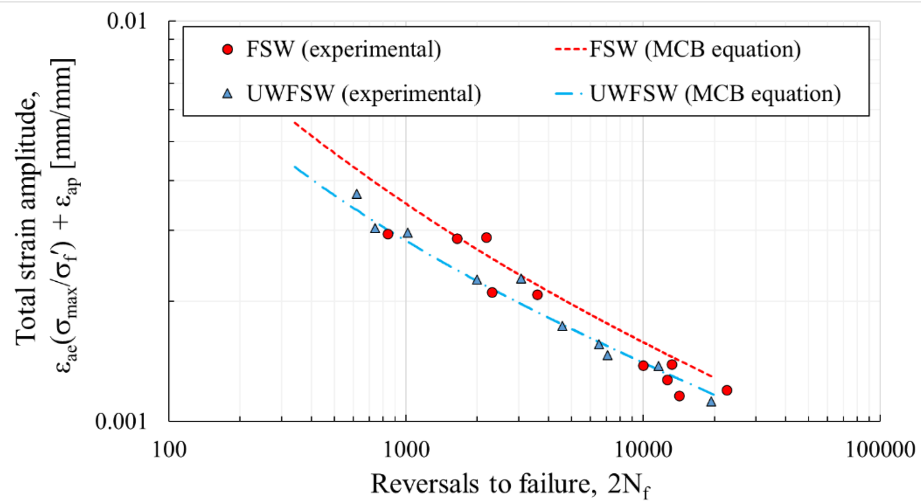

Fig. 3. Fatigue strain-life curves for FSW and UWFSW joints

The curves shown in Fig. 3 are described by the following formula (1), with the determined parameters summarized in Table 4.

$$\varepsilon_{eq,ac} = \frac{\sigma'_f}{E}(2N_f)^{2b} + \varepsilon'_f(2N_f)^c \quad (1)$$

where: σ'_f – fatigue strength coefficient, b – fatigue strength exponent, ε_f – fatigue ductility coefficient, c – fatigue ductility coefficient.

Table 4. *Established values of Manson-Coffin-Basquin relationship components* [13].

Sample	σ'_f	E	b	ε_f	c
FSW	923.4 MPa	70 GPa	-0.122	0.1971	-0.757
UWFSW	940.6 MPa		-0.125	0.2984	-0.95

To evaluate the accuracy of lifetime prediction for FSW and UWFSW joints, results from selected samples were plotted in the graphs shown in Fig. 4.

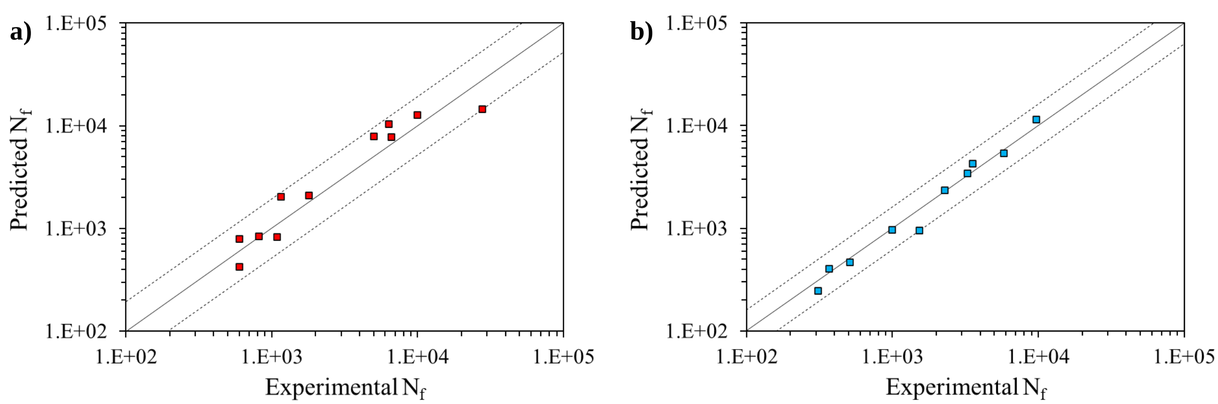

Fig. 4. Life prediction results for FSW (a) and UWFSW (b) joints

Dispersion bands and the standard deviation values for both joint variants were determined using the formula (2) below, with the complete data summarized in Table 5.

$$S = \sqrt{\left[\frac{1}{n-1}\sum_{i=1}^{n}\left(lgN_{pre} - lgN_{exp}\right)^2\right]} \tag{2}$$

where: N_{pre} – predicted lifetime, N_{exp} – experimental lifetime.

Table 5. *Evaluation of lifetime prediction*

Sample	Standard deviation	Dispersion band
FSW	0.0135	1.93
UWFSW	0.0035	1.61

The obtained results indicate that the Manson-Coffin-Basquin equation provides a good prediction of the fatigue life of FSW and UWFSW joints of the AA7075-T651 alloy. UWFSW joints are characterized by significantly lower standard deviation and narrower dispersion band compared to conventional FSW joints.

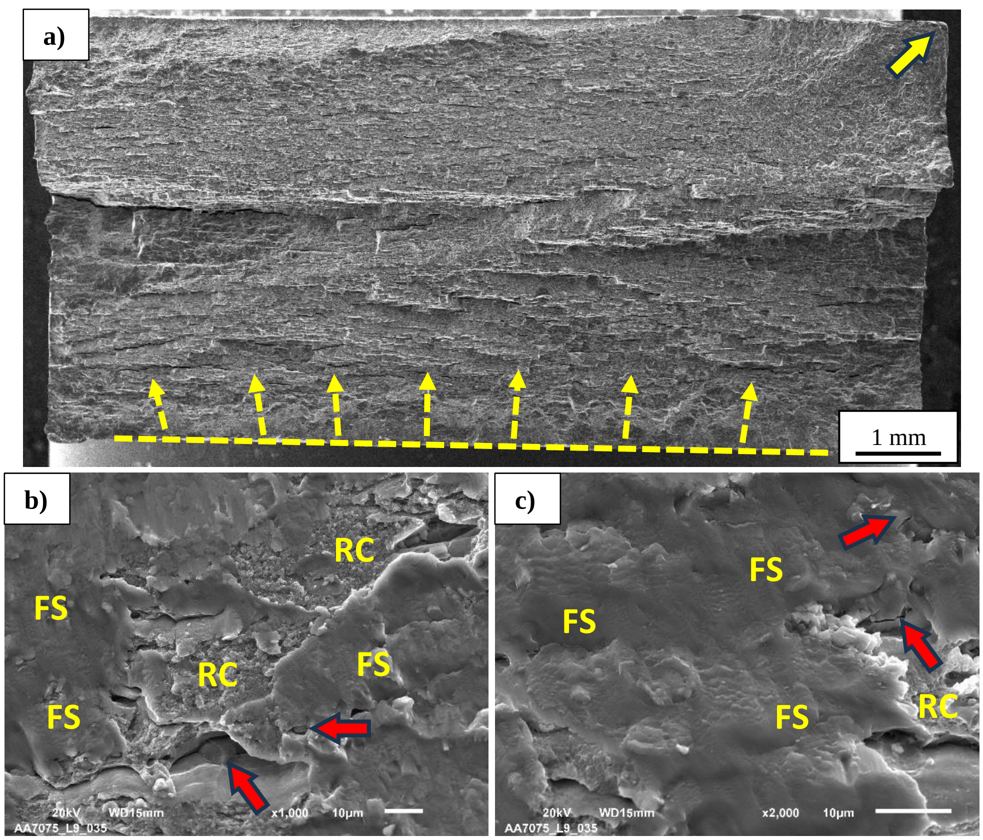

Fig. 5. Results of fractographic examination of AA7075 alloy subjected to LCF under ε_{ac} = 0.35%; general view (a), micro areas with reduced cohesion (b), smooth surface with fatigue strations (c)

After undergoing low cycle fatigue tests, selected samples were subjected to electron-optical examinations of the fatigue fractures using a scanning electron microscope JSM-6610. First, fractographic studies of the samples made from the base material AA7075-T651 were conducted. The results of the observations obtained are presented in Figure 5. The overall view of the fatigue fracture is presented in Figure 5a. The yellow dashed line along with the arrows illustrates the primary direction of the fatigue crack propagation, while the single arrow indicates an additional site of crack initiation. One can observe the influence of texture on the nature of crack propagation, which is manifested in layering with numerous offsets. Observations made at higher magnification in two different places, shown in Figures 5b and 5c, reveal more details, specifically that cracking occurs in a ductile manner with areas of quasi-brittle fracture.

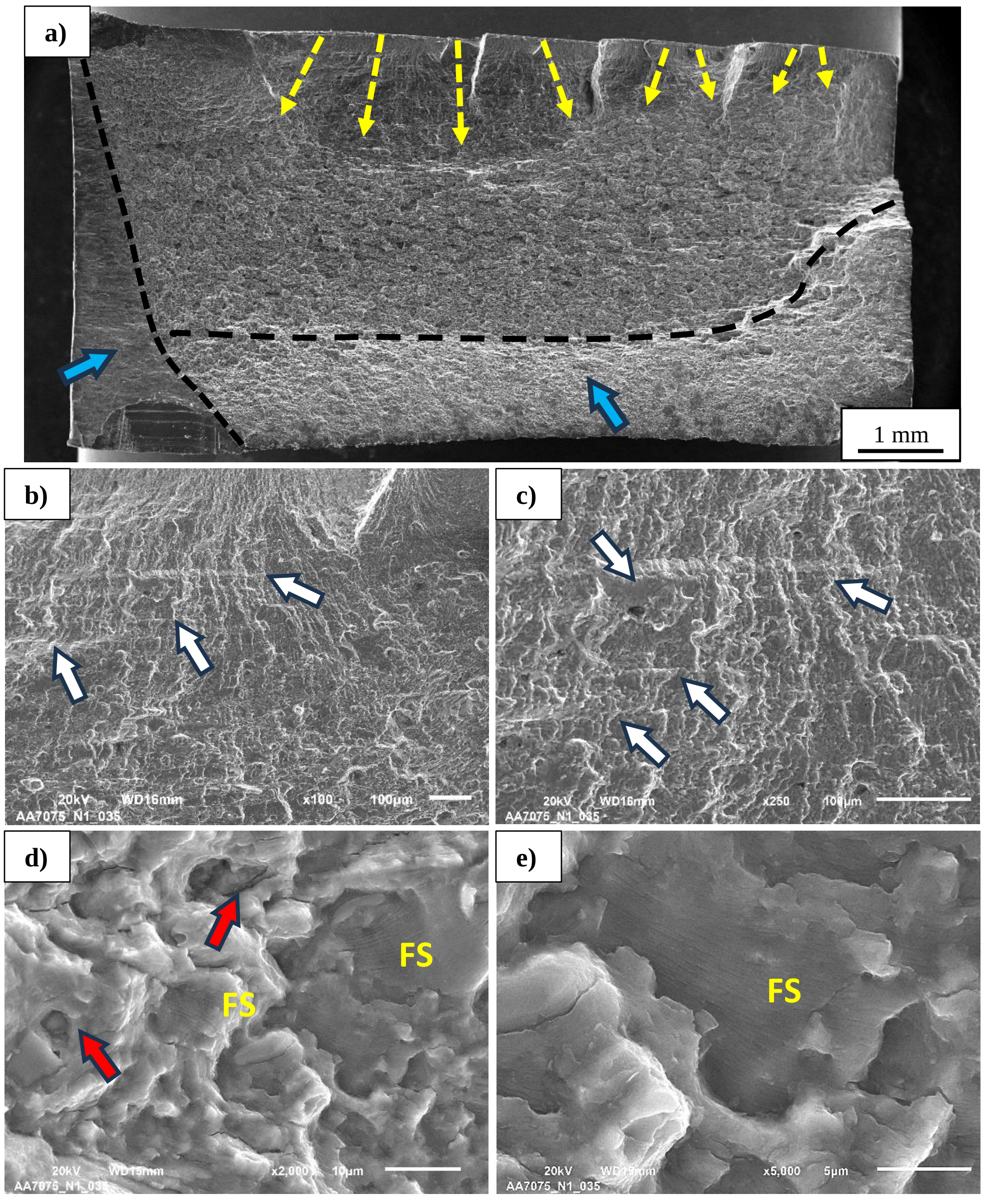

Fig. 6. The fatigue fracture surface of AA7075 alloy FSW joint subjected to LCF under ε_{ac}=0.35%; general view (a), area of stable growth (b,c), details of the fracture surface (d,e)

The smoothed surfaces with fatigue striations (FS) indicate regions of ductile fracture through structural grains. In contrast, micro areas with reduced cohesion (RC) appear at grain boundaries, where numerous microprecipitates degrade the material's continuity. Additionally, larger precipitates, marked with red arrows, contribute to strengthening the material's properties and slow down crack propagation by dispersing energy, leading to crack growth around the inclusion and its decohesion.

Fractographic studies were then conducted on AA7075-T651 material with a FSW joint and the results are presented in Figure 6. At the outset, it should be noted that cracks in the FSW joint samples initiated on both sides of the joint (advancing and retreating), at the periphery of the weld, or in the thermo-mechanically affected zone. Moreover, at high loads, measured by total strain, crack initiation, and propagation also occurred on the root side.

Figure 6a shows the view of the entire fracture surface, indicating the direction of the development of multiple fatigue cracks during the stable crack growth phase (yellow arrows) and the areas of dominant shear (cyan arrows). The black dashed line indicates the area of transition between the zone of fracture due to the exceedance of normal stresses and that obtained as a result of slipping. The area indicated by the cyan arrow was damaged abruptly due to maximum shear stresses in the plane of the easiest slip. Figures 6b and 6c illustrate the area of stable crack growth, where the influence of the material's texture was observed in the form of lighter bands (pointed by white arrows). These are locations where secondary cracks were mostly observed, perpendicular to the observed surface. Figures 6d and 6e show details of the fracture surface where there are pointed fatigue striations (FS) and revealed precipitations (red arrows). The observed spatial, complex structure of the fracture surface indicates a high degree of grain refinement and a ductile fracture character. It is proof that this material has undergone significant plastic deformation before failure, which is also indicative of good toughness and energy absorption capabilities.

In all cases subjected to electron-optical observations, fatigue cracks propagated on the advancing side, which is different than in the vast majority of known or observed cases. At low loads, cracks appeared in the weld near the TMAZ, in contrast to higher loads when cracking originated in the TMAZ or HAZ zone. This is due to the reduction of the effect of the geometric notch, in the form of characteristic arched surface irregularities, with increasing stresses. Furthermore, it was observed that at the highest loads, the crack propagated along the TMAZ. Figures 7 and 8 present the results of the fatigue fracture studies of the FSW joint performed in water conditions (UWFSW) tested at a load ε_{ac} of 0.5% and 0.35%, respectively.

A general view of the fatigue fracture is shown in Figure 7a, where the fatigue crack initiation locations are indicated. Cracking started in the TMAZ zone near the HAZ. The site of crack initiation and the initial stage of cracking are shown in more detail in Figure 7b. During image analysis, regular stripes were observed, repeating approximately every 0.1-0.2 mm, which is probably the result of the welding process. Closer observation (Figure 7c) revealed the presence of numerous regions characterized by different electron-optical properties (dark fields). EDS analysis revealed a high oxygen content, indicating the presence of aluminum oxides. Observations made at high magnifications (Figures 7d and 7e) revealed that these areas have a structure similar to amorphous and are probably grain boundaries revealed during cracking. This can be evidenced by two areas marked in Figure 7d with red arrows, between which there are grains with clearly visible fatigue striations (FS). These surfaces can directly influence the crack growth rate because they reduce the cohesion of the material.

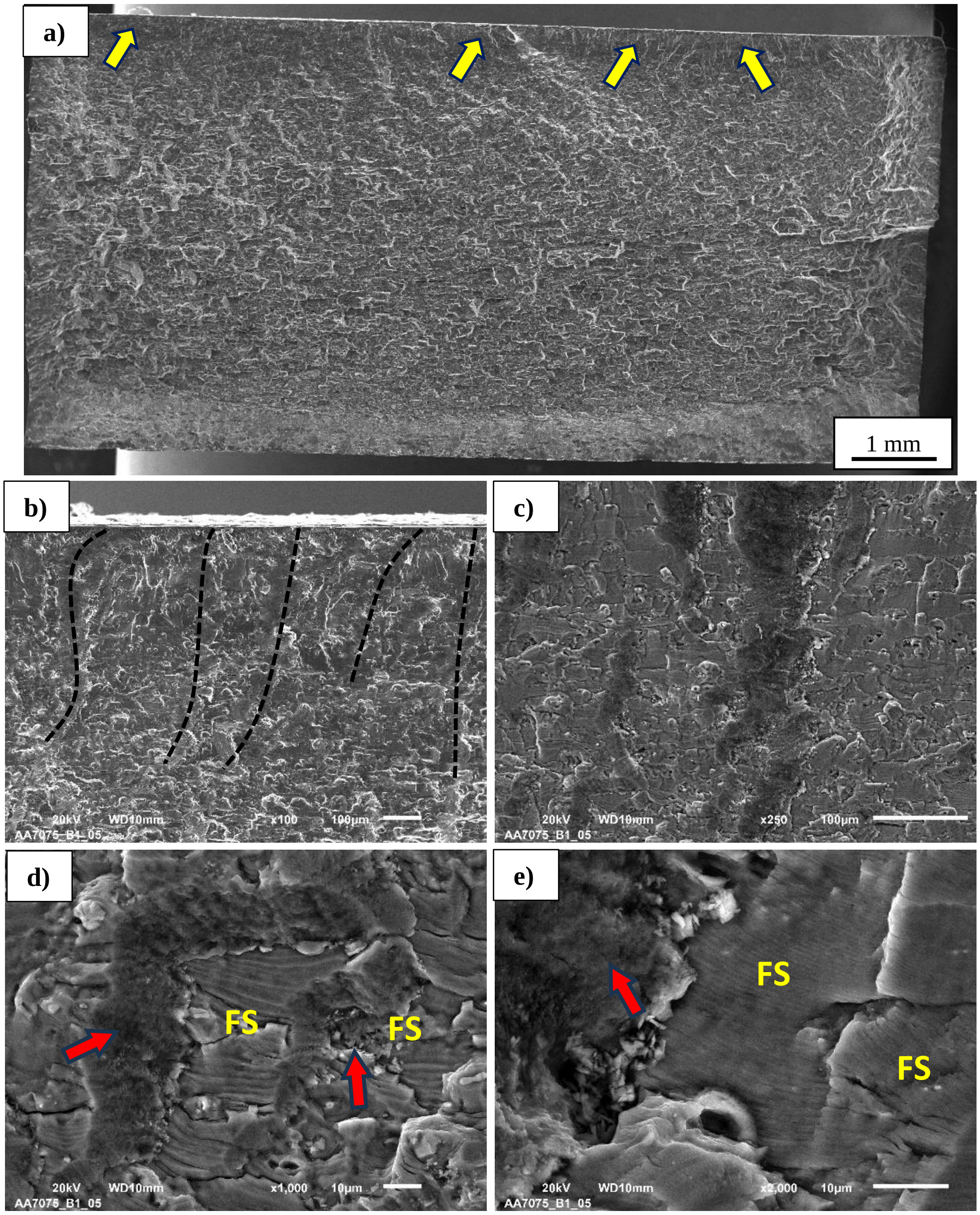

Fig. 7. The fracture surface of UWFSW joints subjected to a load ε_{ac}=0.5%; general view (a), crack initation site (b), bands with aluminum oxide (c,d), magnification of fatigue striations close to the oxide-containing bands (e)

Then, the fracture surface of the sample examined at a load εac of 0.35% was analyzed, the view of which is shown in Figure 8a. In this case, cracks are initiated from surface imperfections located in the weld, close to the TMAZ, and the two main origins are marked with arrows. In the central area of the crack, a region with characteristic dark stripes was observed, which is marked with a dashed line. In these dark areas, the phenomenon described earlier occurred and its description is therefore omitted.

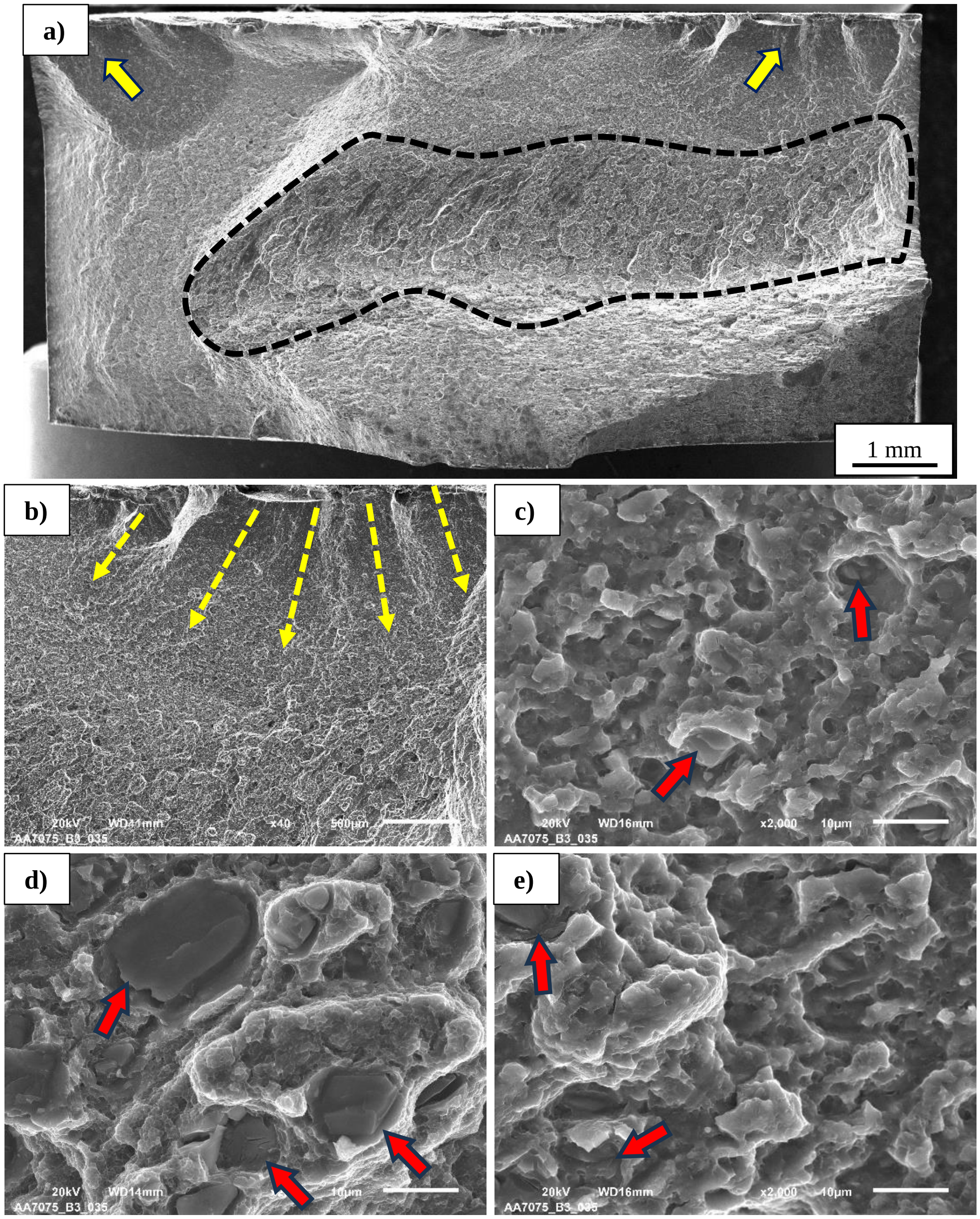

Fig. 8. The fracture surface of UWFSW joints subjected to a load ε_{ac}=0.35%; general view (a), crack initation site (b), magnification of fracture surface morphology (c), large precipitates (d,e)

Figure 8b shows the dynamic character of crack initiation, which occurred simultaneously in many places. The following photos (Figures 8c, d, and e) show the fracture surface morphology at high magnification. Importantly, fatigue striations were not observed anywhere at any stage of fracture. The presented images clearly indicate the ultrafine-grained structure of the material with numerous precipitates (red arrows) of various sizes. The cracking develops both around these precipitates and often causes their brittle cracking, which indicates a very strong cohesion of the precipitates with the matrix. The observed fracture behavior is similar to typical microvoid coalescence, with the formation of characteristic fine dimples, widely reported in scientific studies on FSW welding of precipitation-hardened alloys [25,26]. The identified bands with an increased concentration of oxide inclusions can be considered regions that reduce the joint's durability. The presence of oxide inclusions in FSW joints may occur, for example, during corner welding, and represents a significant issue affecting the joint's strength [27]. Further research is required to determine whether the UWFSW process may promote an increase in the occurrence of such inclusions in the stir zone.

CONCLUSIONS

The following conclusions can be drawn from this study:

- The analysis of the obtained hysteresis loops revealed that FSW joint exhibits cyclic hardening, with a stable maximum stress and a decreasing minimum stress, leading to an increased contribution of compressive stresses and a lower mean stress during stabilized fatigue. In comparison, the UWFSW joint also shows cyclic hardening but with a greater contribution of tensile stresses, a higher mean stress, and a reduced participation of plastic deformation.
- The Manson-Coffin-Basquin equation effectively predicts the fatigue life of AA7075-T651 alloy joints, with UWFSW joints exhibiting significantly lower standard deviation and narrower dispersion bands compared to conventional FSW joints.
- The fracture behavior of UWFSW joints, occurring in the TMAZ, is similar to the characteristic ductile fracture mode observed in precipitation-hardened aluminum alloys. At the same time, fracture surface analysis revealed the presence of aluminum oxide dispersion in the stir zone, which was likely introduced into the material during the welding process.
-

ACKNOWLEDGEMENT

This work was financed by Military University of Technology under research project UGB 708/2024.

Conflicts of Interest: The authors declare that they have no competing financial interests or personal relationships that could have seemed to influence the study reported in this paper.

REFERENCES

1. Çam G., Mistikoglu S. Recent developments in friction stir welding of Al-alloys. J. Mater. Eng. Perform. 2014, 23, 1936–1953. https://doi.org/10.1007/s11665-014-0968-x
2. Li D., Yang X., Cui L., He Fa., Zhang X. Investigation of stationary shoulder friction stir welding of aluminum alloy 7075-T651. Journal of Materials Processing Technology, 2015, 222. https://doi.org/10.1016/j.jmatprotec.2015.03.036

3. Kosturek R., Torzewski J., Wachowski M., Śnieżek L. Effect of Welding Parameters on Mechanical Properties and Microstructure of Friction Stir Welded AA7075-T651 Aluminum Alloy Butt Joints. Materials 2022, 15, 17, 5950. https://doi.org/10.3390/ma15175950
4. Mahoney M.W., Rhodes C.G., Flintoff J.G. et al. Properties of friction-stir-welded 7075 T651 aluminum. Metall Mater Trans A 1998, 29, 1955–1964. https://doi.org/10.1007/s11661-998-0021-5
5. Joshi A., Gope A., Gope P.C. Effect of post-weld heat treatment on mechanical properties and fatigue crack growth behaviour of friction stir welded 7075-T651 Al alloy. Theoretical and Applied Fracture Mechanics 2023, 123, 103714. https://doi.org/10.1016/j.tafmec.2022.103714
6. Wahid M.A., Khan Z.A., Siddiquee A.N. Review on underwater friction stir welding: A variant of friction stir welding with great potential of improving joint properties. Trans. Nonferrous Met. Soc. China 2018, 28, 2, 193-219. https://doi.org/10.1016/S1003-6326(18)64653-9
7. Liu H.J., Zhang H.J., Yu L. Effect of welding speed on microstructures and mechanical properties of underwater friction stir welded 2219 aluminum alloy. Materials & Design 2011, 32, 3, 1548-1553. https://doi.org/10.1016/j.matdes.2010.09.032
8. Sree Sabari S., Malarvizhi S., Balasubramanian V. Characteristics of FSW and UWFSW joints of AA2519-T87 aluminium alloy: Effect of tool rotation speed. Journal of Manufacturing Processes 2016, 22, 278-289. https://doi.org/10.1016/j.jmapro.2016.03.014
9. Iwaszko J., Kudła K. Evolution of Microstructure and Properties of Air-Cooled Friction-Stir-Processed 7075 Aluminum Alloy. Materials 2022, 15, 7, 2633. https://doi.org/10.3390/ma15072633
10. Rouzbehani R., Kokabi A.H., Sabet H., Paidar M., Ojo O.O. Metallurgical and mechanical properties of underwater friction stir welds of Al7075 aluminum alloy. Journal of Materials Processing Technology 2018, 262, 239-256. https://doi.org/10.1016/j.jmatprotec.2018.06.033
11. Janeczek A., Tomków J., Derazkola H., Łyczkowska K., Fydrych D. Effect of underwater friction stir welding parameters on AA5754 alloy joints: experimental studies. The International Journal of Advanced Manufacturing Technology 2024, 134, 5643-5655. 10.1007/s00170-024-14485-9.
12. Sabari S., Malarvizhi S., Balasubramanian V. Influences of tool traverse speed on tensile properties of air cooled and water cooled friction stir welded AA2519-T87 aluminium alloy joints. Journal of Materials Processing Technology 2016, 237. https://doi.org/10.1016/j.jmatprotec.2016.06.015
13. Kosturek R., Torzewski J., Śnieżek L. Study on Underwater Friction Stir Welding of AA7075-T651. Advances in Science and Technology Research Journal 2024, 18, 8, 191-203. https://doi.org/10.12913/22998624/193529
14. Pedapati S. R., Paramaguru D., Awang M., Mohebbi H., Korada S. Effect of process parameters on mechanical properties of AA5052 joints using underwater friction stir welding. Journal of Mechanical Engineering and Sciences 2020, 14. 6259-6271. 10.15282/jmes.14.1.2020.05.0490.
15. Kumar S., Thangaraju R., Pandey S., Sirohi S., Pandey C. Effects of welding parameter on the microstructure and mechanical properties of friction stir-welded non-heat treatable alloy AA5083. Journal of Adhesion Science and Technology 2024, 1-19. 10.1080/01694243.2024.2406567.
16. Sasikumar A., Gopi S., Mohan D.G. Prediction of Filler Added Friction Stir Welding Parameters for Improving Corrosion Resistance of Dissimilar Aluminium Alloys 5052 and 6082 Joints. Advances in Materials Science, 2022, 22, 3, 79-95. https://doi.org/10.2478/adms-2022-0014

17. Xu W.F., Liu J.H., Chen D.L., Luan G.H. Low-cycle fatigue of a friction stir welded 2219-T62 aluminum alloy at different welding parameters and cooling conditions. Int J Adv Manuf Technol 2014, 74, 209-218. https://doi.org/10.1007/s00170-014-5988-z

18. Zhang J., Upadhyay P., Hovanski Y., Field D. High-Speed Friction Stir Welding of AA7075-T6 Sheet: Microstructure, Mechanical Properties, Micro-texture, and Thermal History. Metallurgical and Materials Transactions A 2017, 49. https://doi.org/10.1007/s11661-017-4411-4

19. Ahmed M. M. Z., El-Sayed Seleman M. M., Fydrych D., Çam G. Review on friction stir welding of dissimilar magnesium and aluminum alloys: Scientometric analysis and strategies for achieving high-quality joints. Journal of Magnesium and Alloys 2023, 11, 11, 4082-4127. https://doi.org/10.1016/j.jma.2023.09.039

20. Feng A.H., Chen D.L., Ma Z.Y. Microstructure and Low-Cycle Fatigue of a Friction-Stir-Welded 6061 Aluminum Alloy. Metall Mater Trans A 2010, 41, 2626–2641. https://doi.org/10.1007/s11661-010-0279-2

21. Iwaszko J. New Trends in Friction Stir Processing: Rapid Cooling—A Review. Transactions of the Indian Institute of Metals, 2022, 75, 1681–1693. https://doi.org/10.1007/s12666-022-02552-2

22. Khalaf H.I., Al-Sabur R., Abdullah M.E., Kubit A., Derazkola H.A. Effects of Underwater Friction Stir Welding Heat Generation on Residual Stress of AA6068-T6 Aluminum Alloy. Materials 2022, 15, 2223. https://doi.org/10.3390/ma15062223

23. Kosturek R., Śnieżek L., Torzewski J., Ślęzak T., Lewczuk R. Influence of post-weld explosive treatment on low cycle fatigue of AA7075-T651 friction stir welded joint. Theoretical and Applied Fracture Mechanics 2024. 133, Part A, 104574. https://doi.org/10.1016/j.tafmec.2024.104574

24. Fu L., Duan H., Li H., Lin L., Wang Q., Yao Ji., Luo Y. Low-cycle fatigue behavior of 7075-T6 aluminum alloy at different strain amplitudes. Materials Express 2020, 10. 942-947. https://doi.org/10.1166/mex.2020.1696.

25. Kumar R., Upadhyay V., Pandey, C. Effect of Post-Weld Heat Treatments on Microstructure and Mechanical Properties of Friction Stir Welding Joints of AA2014 and AA7075. J. of Materi Eng and Perform, 2023, 32, 10989–10999. https://doi.org/10.1007/s11665-023-07927-0

26. Kubit A., Derazkola H.A., Myśliwiec, P. et al. Effects of polymer sealant interlayer on quality of EN AW-2024-T3 aluminum alloy lap joint prepared by friction stir welding. Arch. Civ. Mech. Eng. 2024, 24, 238. https://doi.org/10.1007/s43452-024-01047-9

27. Mertinger V., Varbai B., Adonyi Y. et al. Microstructure evaluation of dissimilar AA2024 and AA7050 aluminum joints made by corner stationary-shoulder friction stir welding. Weld World 2022, 66, 1623–1635. https://doi.org/10.1007/s40194-022-01321-5